Chromium Oxide Complexes with Dinitrogen. Formation and Characterization of the $(NN)_xCrO$ and $(NN)_xCrO_2$ ($x = 1,2$)

Mingfei Zhou,* Luning Zhang, and Qizong Qin

Department of Chemistry, Laser Chemistry Institute, Fudan University, Shanghai 200433, P. R. China

Received: January 16, 2001; In Final Form: April 20, 2001

Matrix isolation infrared spectra and quantum chemical calculations of the $(NN)_xCrO$ and $(NN)_xCrO_2$ ($x = 1$, 2) molecules are reported. These species were prepared and isolated in solid argon by three different methods: co-condensation of the CrO and CrO_2 molecules generated from laser ablation of CrO_3 with N_2/Ar; reactions of laser-ablated Cr atoms with O_2/N_2/Ar mixtures, and reactions of laser-ablated Cr atoms with N_2O/Ar. The product absorptions were identified by isotopic substitutions and density functional theoretical calculations. Evidence is also presented for the $(NN)(O_2)CrO_2$ molecule.

Introduction

Activation of the N−N triple bond and its chemical transformations is one of the most challenging subjects in chemistry.[1,2] The N−N triple bond in a bare N_2 molecule has a high bond energy of 225.94 kcal/mol, which makes the cleavage of the N−N bond very difficult. Dinitrogen binding to the electron-rich metal centers elongates the N−N bond and makes it potentially activable. Many studies have indicated that a coordinated dinitrogen is reactive to a variety of reagents to generate N−H and N−C bonds. Since the report of the first transition metal dinitrogen complex, there have been hundreds of different transition metal−dinitrogen complexes characterized.[3−6]

Dinitrogen complexes of chromium have received considerable attention. Reactions of chromium metal atoms with dinitrogen molecules have been studied both experimentally and theoretically.[7−10] Binary chromium dinitrogen complexes with from one to six N_2 molecules have been synthesized in low-temperature matrices.[7,8] Chromium metal complexes containing dinitrogen together with various ligands, such as CO, C_6H_6, and PR_3 have also been studied.[11−14] The $Cr(CO)_5N_2$ complex is thermally stable only in a solution of liquid xenon.[12] Phosphine ligands stabilize N_2 complexes, the observed Cr−N_2 bond length in a phosphine complex of Cr is significantly shorter than that for $Cr(CO)_5N_2$.[13]

Matrix-isolation-infrared spectroscopy has proved to be an effective method for characterization of transition metal complexes with weakly bound ligands. Recent investigations of laser-ablated transition metal halides with small molecules have characterized a series of novel transition metal complexes in a solid argon matrix.[15−17] In this paper, we report a study of combined matrix-isolation FTIR spectroscopic and density functional theoretical study on the dinitrogen complexes of chromium mono- and dioxides. These dinitrogen complexes can be generated from reactions of laser-ablated chromium oxides with N_2 or chromium atoms with $O_2 + N_2$ mixture or N_2O molecules in solid argon.

* Corresponding author. E-mail: mfzhou@fudan.edu.cn. Fax: +86-21-65102777.

Experimental and Theoretical Methods

The experimental setup was similar to that described previously.[18] The 1064 nm Nd:YAG laser fundamental (Spectra Physics, DCR 2, 20 Hz repetition rate and 8 ns pulse width) was focused onto a rotating target (CrO_3 or Cr) through a hole in a CsI window. Typically, 5−10 mJ/pulse laser power was used. The ablated species were codeposited with reagent gases in excess argon onto the 11 K CsI window at a rate of 5 mmol/h. The CsI window was mounted on a copper holder at the cold end of the cryostat (Air Products Displex DE202) and maintained by a closed-cycle helium refrigerator (Air Products Displex IR02W). A Bruker IFS 113v FTIR spectrometer equipped with a DTGS detector was used to record the IR spectra in the range of 400−4000 cm^{-1} with a resolution of 0.5 cm^{-1}. Matrix samples were annealed at different temperatures, and selected samples were subjected to broadband photolysis using a 250 W high-pressure mercury lamp.

Density functional calculations were carried out using the Gaussian 98 program.[19] The Becke's three-parameter hybrid equation with the Lee−Yang−Parr correlated functional (B3LYP) was used.[20,21] We introduced the standard Wachters−Hay all electron basis set on Cr and the 6-311+G(d) on N and O atoms.[22,23] Structures were fully optimized with consecutive calculation of the harmonic vibrational frequencies using analytical second derivatives. Population analysis was carried out using the NBO method.[24]

Results

$CrO_3 + N_2$/Ar. Experiments were done using a CrO_3 target. Co-condensation of laser-ablated oxides with pure argon forms CrO_2 (965.3 and 914.3 cm^{-1}) as the major product with minor CrO (846.8 cm^{-1}), CrO_3 (968.4 cm^{-1}), CrOCrO (984.2 cm^{-1}), and Cr_2O_2 (716.1 and 642.9 cm^{-1}).[25,26] These absorptions showed no obvious change on annealing. New product absorptions were observed when different concentration N_2/Ar mixtures were used as the reagent gas. The spectra in the 2330−2130 and 980−830 cm^{-1} regions are shown in Figure 1, with the product absorptions listed in Table 1. Note the evolution of bands as the sample was subsequently annealed to 25 and 30

10.1021/jp0101514 CCC: $20.00
Published on Web 06/07/2001

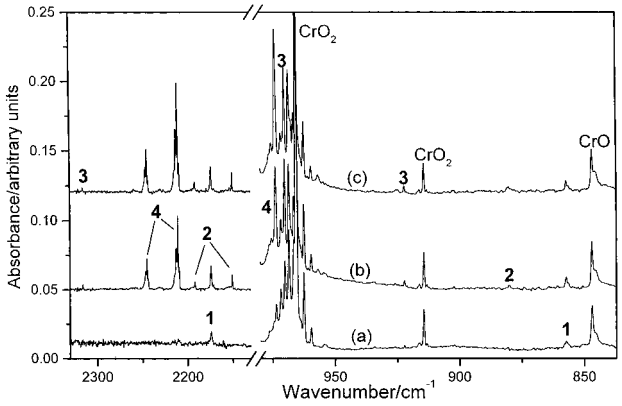

Figure 1. Infrared spectra in the 2330−2130 and 980−830 cm^{-1} regions for laser-ablated CrO_3 codeposited with 0.2% N_2 in argon at 11 K: (a) 1 h sample deposition; (b) after 25 K annealing; (c) after 30 K annealing. Key: **1**, NNCrO; **2**, $(NN)_2CrO$; **3**, $NNCrO_2$; **4**, $(NN)_2CrO_2$.

K. After deposition, two weak bands at 857.2 and 2173.8 cm^{-1} were observed. These absorptions increased together on 25 K annealing. Annealing at 25 K also produced three new band sets at 2316.0, 970.0, 922.2 cm^{-1}, 2245.0, 2210.8, 973.8 cm^{-1}, and 2191.8, 2150.3, 880.3 cm^{-1}. Further annealing to 30 K decreased the 2316.0, 970.0, 922.2 cm^{-1} band set and increased the 2245.0, 2210.8, 973.8 cm^{-1} and 2191.8, 2150.3, 880.3 cm^{-1} band sets. Experiments were done with the $^{15}N_2$/Ar sample; the absorptions in the 2330−2130 cm^{-1} region were shifted as given in Table 1. The spectra in the 980−830 cm^{-1} region were identical with the $^{14}N_2$ spectra. Identical laser-ablation investigations were done with mixed $^{14}N_2 + {}^{15}N_2$ and $^{14}N_2 + {}^{14}N^{15}N + {}^{15}N_2$ samples. Figure 2 illustrates the spectra in the 2330−2060 cm^{-1} region using a 0.3% $^{14}N_2$ + 0.3% $^{15}N_2$ sample. Pure isotopic counterparts were observed for the 2316.0 and 2173.8 cm^{-1} bands, and triplets were produced for the 2245.0, 2210.8, 2191.8, and 2150.3 cm^{-1} bands, as also listed in Table 1. Figure 3 shows the spectra in the 2260−2060 cm^{-1} region using a 0.15% $^{14}N_2$ + 0.3% $^{14}N^{15}N$ + 0.15% $^{15}N_2$ sample. The initial sample deposit showed a triplet at 2173.8, 2138.2, and 2101.8 cm^{-1}. Compared with the spectra shown in Figure 2, extra strong new intermediates at 2234.6, 2197.3, 2184.5, and 2147.3 cm^{-1} were observed for the 2245.0 and 2210.8 cm^{-1} bands on annealing.

Cr + O_2/N_2/Ar. Figure 4 shows the spectra in the Cr−O stretching vibrational frequency region from codeposition of laser-ablated Cr atoms with 0.5% N_2 + 0.5% O_2 in argon. Sample deposition produced strong CrO_2 (965.3, 914.3 cm^{-1}), $(O_2)CrO_2$ (973.8, 918.2 cm^{-1}),[27] and O_4^- (953.8 cm^{-1}) absorptions.[28] Annealing decreased the $(O_2)CrO_2$ and O_4^- absorptions and produced new absorptions at 970.0, 967.5, 922.2, 2316.0, 2245.0, and 2210.8 cm^{-1}. A similar experiment using 0.5% N_2 + 0.5% $^{18}O_2$ in argon was also done, and the spectra are also shown in Figure 4. All absorptions in the Cr−O stretching vibrational frequency region exhibited an oxygen isotopic shift, as also listed in Table 1. It can be seen from Figure 4 that the 973.8 cm^{-1} band split into two bands at 937.6 and 936.8 cm^{-1} in $^{18}O_2$ spectra, indicating that there are two components under the 973.8 cm^{-1} band. The 936.8 cm^{-1} band was due to $(O_2)Cr^{18}O_2$ absorption, and the 937.6 cm^{-1} band went together with the 2245.0 and 2210.8 cm^{-1} bands. The 936.8 cm^{-1} band decreased on annealing, while the 937.6 cm^{-1} band increased on annealing.

An additional Cr + 0.5% O_2/Ar experiment was done. Sample deposition produced CrO_2, $(O_2)CrO_2$, and O_4^- absorptions. Annealing decreased the $(O_2)CrO_2$ absorptions and produced the $(O_2)_2CrO_2$ (1153.9, 1134.2, 971.4 cm^{-1})[27] and CrO_3 (968.4 cm^{-1}) absorptions. However, the 970.0, 967.5, 922.2, 2316.0, 2245.0, and 2210.8 cm^{-1} absorptions were not observed.

Cr + N_2O/Ar. A supplemental experiment was done with a Cr metal target and 0.2% N_2O in argon, and the spectra in the Cr−O stretching vibrational frequency region are shown in Figure 5. After deposition, two bands at 2173.8 and 857.2 cm^{-1} were observed together with the CrO absorption at 846.8 cm^{-1} and very weak CrO_2 absorption at 965.3 cm^{-1}. The 2245.0, 2210.8, 973.8 cm^{-1} and 2316.0, 970.0, 922.2 cm^{-1} band sets increased on 25 K annealing. Mercury arc photolysis slightly decreased the 2245.0, 2210.8, 973.8 cm^{-1} band set and increased the 2316.0, 970.0, 922.2 cm^{-1} and 2173.8, 857.2 cm^{-1} band sets. Another 30 K annealing produced a very weak band set at 880.3, 2191.8, 2150.3 cm^{-1}.

TABLE 1: Infrared Absorptions (cm^{-1}) from Codeposition of Laser-Ablated CrO_2 with N_2/Ar or Cr with O_2/N_2/Ar

$^{14}N_2$	$^{15}N_2$	$^{18}O_2$	$^{14}N_2 + {}^{15}N_2$	assignment (mode)
2316.0	2238.7	2316.0	2316.0, 2238.7	$NNCrO_2$ N−N
2245.0	2170.3	2245.0	2245.0, 2231.6, 2170.3	$(NN)_2CrO_2$ sym N−N
2210.8	2137.2	2210.8	2210.8, 2150.1, 2137.2	$(NN)_2CrO_2$ asym N−N
2191.8	2119.0		2191.8, 2176.8, 2119.0	$(NN)_2CrO$ sym N−N
2173.8	2101.8		2173.8, 2101.8	NNCrO N−N
2150.3	2079.0		2150.3, 2093.6, 2079.0	$(NN)_2CrO$ asym N−N
1153.9	1153.9	1090.6		$(O_2)_2CrO_2$ sym O−O
1134.2	1134.2	1070.8		$(O_2)_2CrO_2$ asym O−O
984.2				CrOCrO Cr−O
973.8	973.8	937.6		$(NN)_2CrO_2$ asym OCrO
973.8	973.8	936.8		$(O_2)CrO_2$ asym OCrO
971.4	971.4	934.5		$(O_2)_2CrO_2$ asym OCrO
970.0	970.0	933.7		$NNCrO_2$ asym OCrO
968.4	968.4			CrO_3 asym OCrO
967.5	967.5	930.8		$(NN)(O_2)CrO_2$ asym OCrO
965.3	965.3	929.2		CrO_2 asym OCrO
		917.6		$(NN)(O_2)CrO_2$ sym OCrO
922.2	922.2	877.7		$NNCrO_2$ sym OCrO
918.2	918.2			$(O_2)CrO_2$ sym OCrO
914.3	914.3	869.6		CrO_2 sym OCrO
880.3	880.3			$(NN)_2CrO$ Cr−O
857.2	857.2			NNCrO Cr−O
846.8	846.8			CrO
716.1	716.1			Cr_2O_2
642.9	642.9			Cr_2O_2

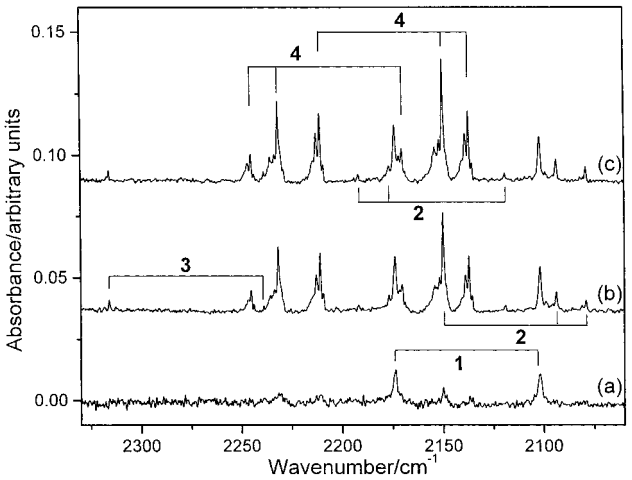

Figure 2. Infrared spectra in the 2330−2060 cm^{-1} region for laser-ablated CrO_3 codeposited with 0.3% $^{14}N_2$ + 0.3% $^{15}N_2$ in argon at 11 K: (a) 1 h sample deposition; (b) after 25 K annealing; (c) after 30 K annealing. Key: **1**, NNCrO; **2**, $(NN)_2CrO$; **3**, $NNCrO_2$; **4**, $(NN)_2CrO_2$.

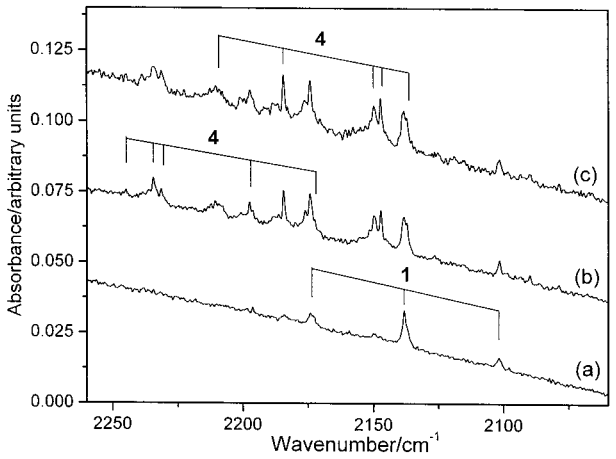

Figure 3. Infrared spectra in the 2260−2060 cm^{-1} region for laser-ablated CrO_3 codeposited with 0.15% $^{14}N_2$ + 0.3% $^{14}N^{15}N$ + 0.15% $^{15}N_2$ in argon at 11 K: (a) 1 h sample deposition; (b) after 25 K annealing; (c) after 30 K annealing. Key: **1**, NNCrO; **4**, $(NN)_2CrO_2$.

Calculation Results. To assist in the identification of the new product absorptions, density functional theoretical calculations were performed. Test calculations were first done on N_2, CrO, CrO_2, and CrO_3, and the results are listed in Table 2. The N_2 bond length and harmonic vibrational frequency were calculated to be 1.096 Å and 2445 cm^{-1}, comparable to the 1.0975 Å and 2359.6 cm^{-1} experimental gas-phase values.[29] In accord with high level CCSD(*t*) calculations,[30] the ground state of CrO was a $^5\Pi$ with Cr−O bond length of 1.616 Å and 868 cm^{-1} harmonic frequency. The CrO_2 was found to have a bent $^3B_1$ ground state with vibrational frequencies at 1032 (υ_3), 989 (υ_1), and 225 cm^{-1} (υ_2). The upper two frequencies were very close to the experimental observed frequencies: 965.3 and 914.3 cm^{-1} in solid argon.[26] The CrO_3 molecule was predicted to have a $^1A_1$ ground state with C_{3v} symmetry.

We optimized both side-on and end-on structures for N_2CrO. Both side-on and end-on structures had quintet ground states. Both the bent and linear end-on structures were more stable than the side-on structure. The bent end-on form of the molecule was the lowest energy structure, although the linear end-on $^5\Pi$ state was only 1.6 kcal/mol higher in energy, it had an imaginary bending frequency. For the $(N_2)_2CrO$ molecule, we only optimized for the end-on structure, and the lowest energy state was a quintet with planar C_{2v} symmetry.

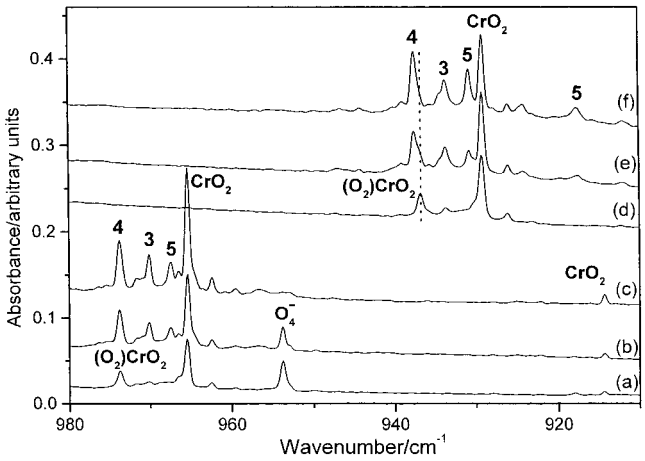

Figure 4. Infrared spectra in the 980−910 cm^{-1} region for laser-ablated Cr atoms codeposited with N_2 + O_2 mixtures in argon at 11 K: (a) 0.5% $^{16}O_2$ + 0.5% N_2, 1 h sample deposition; (b) after 25 K annealing; (c) after 30 K annealing; (d) 0.5% $^{18}O_2$ + 0.5% N_2, 1 h sample deposition; (e) after 25 K annealing; (f) after 30 K annealing. Key: **3**, $NNCrO_2$; **4**, $(NN)_2CrO_2$; **5**, $(NN)(O_2)CrO_2$.

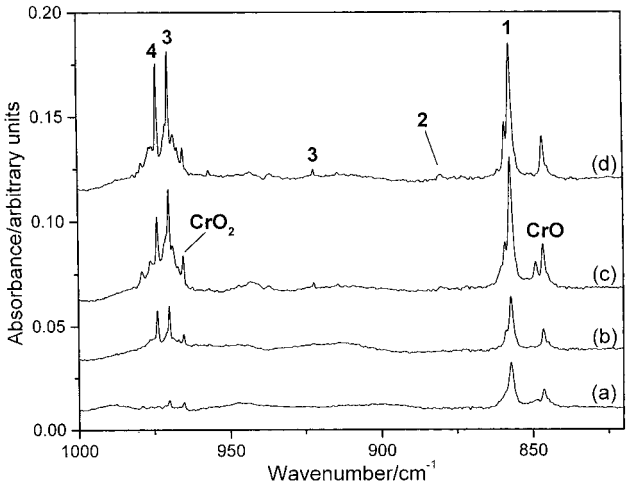

Figure 5. Infrared spectra in the 1000−820 cm^{-1} region for laser-ablated Cr atoms codeposited with 0.2% N_2O in argon at 11 K: (a) 1 h sample deposition; (b) after 25 K annealing; (c) 20 min broadband photolysis; (d) after 30 K annealing. Key: **1**, NNCrO; **2**, $(NN)_2CrO$; **3**, $NNCrO_2$; **4**, $(NN)_2CrO_2$.

TABLE 2: Calculated Geometric Parameters, Vibrational Frequencies (cm^{-1}), and Intensities (km/mol) for the N_2, CrO, CrO_2, and CrO_3

molecule	geometry	frequency (intensity)
N_2 ($^1\Sigma_g^+$)	1.096	2445 (0)
CrO ($^5\Pi$)	1.616	868 (173)
CrO ($^5\Sigma^+$)	1.649	897 (220)
CrO_2 ($^3B_1$)	1.598, 132.0	1032 (488, b_1), 989 (24, a_1), 225 (42, a_1)
CrO_2 ($^1A_1$)	1.589, 127.0	1033 (462, b_1), 1032 (20, a_1), 243 (51, a_1)
CrO_3 ($^1A_1$)	1.578, 115.4	1077 (480, e), 1003 (6, a_1), 376 (0,e), 202 (81,a_1)

Similarly, geometry optimizations of the end-on and side-on structures of N_2CrO_2 indicated that the end-on structure was more stable than the side-on structure. The lowest energy state of $NNCrO_2$ was a triplet with T-shaped C_{2v} symmetry. For the $(NN)_2CrO_2$ molecule, geometry optimization found a $^1A_1$ singlet ground state with pseudotetrahedral C_{2v} structure. The $(NN)(O_2)CrO_2$ molecule was also predicted to have a $^1A'$ ground state. For both $(NN)_2CrO_2$ and $(NN)(O_2)CrO_2$, geometry optimization on the triplet surface converged to triplet $NNCrO_2$ + N_2 or $(O_2)CrO_2$ + N_2.

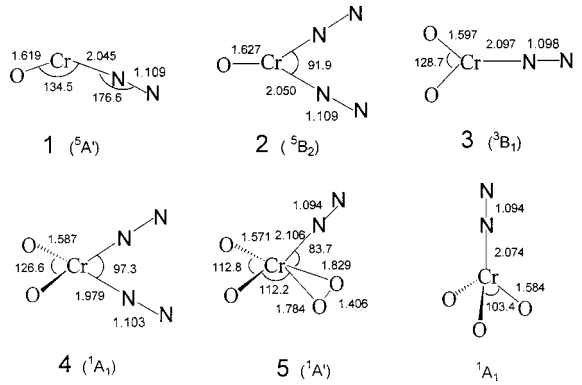

Figure 6. Optimized structures of $(NN)_xCrO$, $(NN)_xCrO_2$ ($x = 1, 2$), $(NN)(O_2)CrO_2$, and $NNCrO_3$ molecules. (Bond lengths are in Ångstroms, and bond angles in degrees).

Calculations were also done on $NNCrO_3$ and also found a $^1A_1$ ground state with C_{3v} symmetry. The optimized structures and geometric parameters for the lowest energy structures of the chromium oxide−dinitrogen complexes are shown in Figure 6, and the vibrational frequencies and intensities are listed in Table 3.

Discussion

NNCrO. The 857.2 and 2173.8 cm^{-1} bands observed in the $CrO_3 + N_2$/Ar experiments after sample deposition increased on 25 K annealing and then decreased on higher temperature annealing. These two bands were the major product absorptions in the $Cr + N_2O$ experiment but were not observed in the $Cr + O_2/N_2$ experiments when CrO was not produced. The 857.2 cm^{-1} band was only 10.4 cm^{-1} blue shifted from CrO observed at 846.8 cm^{-1} in argon and was tentatively assigned to the Cr−O stretching vibration of the NNCrO molecule.[26] The 2173.8 cm^{-1} band shifted to 2101.8 cm^{-1} with $^{15}N_2$ and gave a characteristic isotopic N−N stretching vibrational frequency ratio of 1.0343. In the mixed $^{14}N_2 + {}^{15}N_2$ experiments, only $^{14}N_2$ and $^{15}N_2$ components were observed, indicating that only one N_2 molecule was involved in this mode. In the mixed $^{14}N_2 + {}^{14}N^{15}N + {}^{15}N_2$ experiment, a 1:2:1 triplet was produced, which suggested that the two N atoms are equivalent. However, our DFT calculations showed that the most stable form of N_2CrO exhibits end-on structure with two nonequivalent N atoms, and the splitting of the N−N stretching vibration of the $^{14}N^{15}NCrO$ and $^{15}N^{14}NCrO$ could hardly be distinguished. Of equally importance, the calculated N−N stretching vibrational frequency of end-on structure (2230 cm^{-1}) fit the observed 2173.8 cm^{-1} value much better than that of the side-on structure (2071 cm^{-1}). Accordingly, we assigned the 2173.8 and 857.2 cm^{-1} bands to the N−N and Cr−O stretching vibrations of the NNCrO molecule. An analogous OCCrO molecule was observed in the $Cr + CO_2$ reactions; the Cr−O stretching frequency for the OCCrO was observed at 866.3 cm^{-1}.[31]

DFT calculations predicted the NNCrO molecule to have a $^5A'$ ground state that correlates to the $^5\Pi$ ground-state CrO. The $^5\Pi$ ground-state CrO molecule had a $(d\delta)^2(s\sigma)^1(d\pi)^1$ configuration. When a N_2 ligand interacted with the CrO molecule in a linear fashion, donation from the N_2 HOMO σ orbital led to destabilization of the Cr-based $s\sigma$ orbitals. The $d\pi$ MO was stabilized by $Cr \rightarrow N_2$ π back-donation. However, the $d\pi$ MO was not stabilized enough to switch the relative stability of the $d\pi$ and $s\sigma$ MO's. Hence, the linear NNCrO had a $^5\Pi$ lowest energy state corresponding to a $(d\delta)^2(s\sigma)^1(d\pi)^1$ configuration. Our DFT calculation showed that a linear $^5\Sigma^+$ state NNCrO with the $(d\delta)^2(d\pi)^2(s\sigma)^0$ configuration was only 5.4 kcal/mol higher in energy than the linear $^5\Pi$ state. For comparison, we note that for CrO, the $^5\Sigma^+$ state was calculated to be 17.7 kcal/mol higher in energy than the $^5\Pi$ ground state. By bending the linear NNCrO molecule to the optimized geometry of $^5A'$ state, the energy was lowered about 1.6 kcal/mol as a consequence of reducing the Cr−NN σ repulsion.

The back-donation of π electrons into the antibonding p_π orbital of N_2 led to a reduction of the N−N stretching vibrational frequency. Our DFT calculation predicted the N−N stretching vibration of the $^5A'$ state NNCrO at 2230 cm^{-1}, ca. 215 cm^{-1} lower than the diatomic N_2 frequency, and just 2.6% higher than the observed value. The Cr−O stretching frequency was calculated at 904 cm^{-1}.

$(NN)_2CrO$. The 2191.8, 2150.3, and 880.3 cm^{-1} bands were produced on annealing in $CrO_3 + N_2$/Ar experiments. These three bands maintained the same relative intensities throughout all the experiments, suggesting that they were due to different vibrational modes of the same molecule. As with NNCrO absorptions, these bands were not observed in the $Cr + N_2/O_2$ experiments when CrO was not present. In the $Cr + N_2O$ experiment, these bands were only produced on higher temperature annealing and the relative yield was very low. These suggested that the bands were also due to a $CrO-N_2$ complex. The 880.3 cm^{-1} band is 33.5 cm^{-1} blue shifted from the CrO absorption, it exhibited no nitrogen-15 isotopic shift, and was due to a Cr−O stretching vibration. The 2191.8 and 2150.3 cm^{-1}

TABLE 3: Calculated Vibrational Frequencies (cm^{-1}) and Intensities (in Parentheses, km/mol) for the Structures Described in Figure 6

NNCrO (^{5}A′)	$(NN)_2CrO$ ($^5B_2$)	$NNCrO_2$ ($^3B_1$)	$(NN)_2CrO_2$ ($^1A_1$)	$(NN)(O_2)CrO_2$ (^{1}A′)	$NNCrO_3$ ($^1A_1$)
2230 (853, a′)	2268 (430, a_1)	2393 (100, a_1)	2355 (140, a_1)	2465 (0.3, a′)	2461 (0, a_1)
904 (270, a′)	2214 (996, b_2)	1029 (423, b_2)	2327 (381, b_2)	1066 (211, a″)	1058 (420, e)
323 (19, a′)	927 (294, a_1)	998 (40, a_1)	1041 (335, b_1)	1056 (151, a′)	1002 (6, a_1)
240 (1, a″)	335 (0, b_1)	314 (0, a_1)	1035 (43, a_1)	1004 (66, a′)	379 (31, a_1)
239 (2, a″)	325 (31, b_2)	259 (2, b_1)	462 (8, a_1)	654 (26, a′)	374 (0, e)
84 (18, a′)	319 (0, a_1)	250 (0, b_2)	392 (12, b_2)	592 (5, a′)	300 (2, e)
	289 (16, a_1)	233 (15, a_1)	359 (0, a_1)	374 (1, a′)	226 (27, a_1)
	243 (0, a_2)	105 (37, b_1)	326 (3, b_1)	337 (11, a′)	104 (2, e)
	233 (2, b_2)	75 (3, b_2)	315 (1, b_2)	326 (0.2, a″)	
	101 (15, b_1)		307 (0, a_2)	316 (16, a′)	
	65 (0, a_1)		275 (13, a_1)	277 (0.5, a″)	
	55 (7, b_2)		149 (20, b_2)	238 (6, a′)	
			117 (0, a_2)	225 (2, a″)	
			115 (1, b_1)	113 (0.1, a″)	
			82 (0.4, a_1)	109 (0, a′)	

TABLE 4: Scaling Factors (Observed Frequency/Calculated Frequency) and Observed and Calculated Isotopic Vibrational Frequency Ratios for the Observed Modes of $(NN)_xCrO$ and $(NN)_xCrO_2$ ($x = 1, 2$) Complexes

		scaling	$^{14}N/^{15}N$		$^{16}O/^{18}O$	
molecule	mode	factor	obs	cal	obs	cal
NNCrO	N−N	0.975	1.0343	1.0350	1.0000	1.0000
	Cr−O	0.948	1.0001	1.0000		1.0447
(NN)2CrO	sym N−N	0.967	1.0344	1.0350	1.0000	1.0000
	asy N−N	0.971	1.0343	1.0350	1.0000	1.0000
	Cr−O	0.950	1.0000	1.0001		1.0443
$NNCrO_2$	N−N	0.968	1.0345	1.0350	1.0000	1.0000
	sym OCrO	0.924	1.0000	1.0000	1.0507	1.0514
	asy OCrO	0.943	1.0000	1.0000	1.0389	1.0394
$(NN)_2CrO_2$	sym N−N	0.953	1.0344	1.0350	1.0000	1.0000
	asy N−N	0.950	1.0344	1.0350	1.0000	1.0000
	sym OCrO			1.0000		1.0503
	asy OCrO	0.935	1.0000	1.0000	1.0386	1.0391

bands shifted to 2119.0 and 2079.0 cm^{-1} with $^{15}N_2$/Ar sample and gave isotopic $^{14}N/^{15}N$ ratios of 1.0344 and 1.0343, respectively. In the mixed $^{14}N_2 + {}^{15}N_2$ experiments, both bands formed triplets at 2191.8, 2176.8, 2119.0 cm^{-1} and 2150.3, 2093.6, 2079.0 cm^{-1}. Clearly, two equivalent N_2 molecules were involved in these two modes. The isotopic structure in the mixed $^{14}N_2 + {}^{14}N^{15}N + {}^{15}N_2$ spectrum was too weak to be resolved due to isotopic dilution. Accordingly, the 2191.8, 2150.3, and 880.3 cm^{-1} bands were assigned to the symmetric and antisymmetric N−N stretching and Cr−O stretching vibrations of the $(NN)_2CrO$ molecule. We note that a 891.0 cm^{-1} band was assigned to the Cr−O stretching mode of the $(CO)_2CrO$ molecule in the Cr + CO_2 experiments based on diatomic isotopic ratio and doublet isotopic structure.[31]

The identification of $(NN)_2CrO$ is supported by DFT calculations. The $(NN)_2CrO$ molecule was calculated to have planar C_{2v} symmetry with the two N_2 groups at an angle of 91.9°. The ground state was a $^5B_2$ state corresponding to $^5A'$ NNCrO + N_2. Our DFT calculations predicted frequencies of 2268 (430), 2214 (996) and 927 cm^{-1} (294 km/mol) for the three observed modes. The calculated N−N bond length of $^5B_2$ $(NN)_2CrO$ (1.109 Å) was the same as that of $^5A'$ NNCrO, and the observed N−N stretching mode of NNCrO (2173.8 cm^{-1}) was almost located at the middle of the symmetric and antisymmetric N−N stretching modes of the $(NN)_2CrO$.

$NNCrO_2$. The bands at 2316.0, 970.0, and 922.2 cm^{-1} were observed in all three reaction systems. They increased together on 25 K annealing and then decreased on 30 K and higher temperature annealing. The 2316.0 cm^{-1} band exhibited a 2238.7 cm^{-1} $^{15}N_2$ counterpart and gave a $^{14}N/^{15}N$ isotopic ratio of 1.0345. With $^{14}N_2 + {}^{15}N_2$, no intermediate component was observed, indicating a N−N stretching vibration with one N_2 involvement. The 970.0 and 922.2 cm^{-1} bands showed no nitrogen isotopic shifts but large oxygen isotopic shifts. The oxygen isotopic ratios (1.0389 and 1.0507) indicated that these two bands were antisymmetric and symmetric OCrO stretching vibrations. These three bands were assigned to the $NNCrO_2$ molecule.

Our DFT calculations for $NNCrO_2$ predicted a $^3B_1$ ground state with the N−N stretching frequency at 2393 cm^{-1} (100km/mol). The symmetric and antisymmetric CrO_2 subunit stretching frequencies were calculated at 1029 cm^{-1} (423 km/mol) and 998 cm^{-1} (40 km/mol). The frequencies, relative intensities, and isotopic shifts were in good agreement with experimental values. As listed in Table 4, the calculated $^{14}N/^{15}N$ isotopic ratio was 1.0350 for the N−N stretching mode, and the $^{16}O/^{18}O$ ratios were 1.0394 and 1.0514 for the antisymmetric and symmetric OCrO modes. Vibrational normal-mode analysis also indicated that there was essentially no coupling between the N−N and OCrO vibrations. As can be seen from Figure 6, the calculated N−N distance in $NNCrO_2$ was 1.098 Å, lengthened by only 0.002 Å compared with that in N_2. The Cr−O distance and ∠OCrO in $NNCrO_2$ were also slightly different from the value for the free CrO_2.

$(NN)_2CrO_2$. Three bands at 2245.0, 2210.8, and 973.8 cm^{-1} increased together on annealing in the $CrO_3 + N_2$ as well as Cr + O_2/N_2 and Cr + N_2O experiments. The two upper bands showed N−N stretching isotopic ratios (1.0344, 1.0344). Both bands gave matching asymmetric triplets at 2245.0, 2231.6, 2170.3 cm^{-1} and 2210.8, 2150.1, 2137.2 cm^{-1} in the mixed $^{14}N_2 + {}^{15}N_2$ experiment. This was indicative of the presence of two equivalent N_2 groups in these two modes. The 973.8 cm^{-1} band showed no nitrogen-15 isotopic shift, and the isotopic $^{16}O/^{18}O$ ratio of 1.0386 indicated that this band was due to an antisymmetric OCrO stretching vibration. Accordingly, these three bands are assigned to the $(NN)_2CrO_2$ molecule. The symmetric OCrO stretching vibration was much weaker than the antisymmetric OCrO stretching mode and might be overlapped by other bands and so could not be identified.

Present DFT calculations predicted a singlet ground state for $(NN)_2CrO_2$, which correlated to $^1A_1$ excited-state CrO_2. The closed-shell $(a_1)^2(b_1)^0$ configuration of the $(NN)_2CrO_2$ singlet was somewhat surprising as the neutral CrO_2 molecule preferred a $^3B_1$ triplet with $(a_1)^1(b_1)^1$ configuration, and the $^1A_1$ singlet CrO_2 was predicted to lie 24.0 kcal/mol higher in energy than the $^3B_1$ state. In like fashion, both the $(CO)_2CrO_2$ and $(H_2)_2$-CrO_2 molecules were predicted to have singlet ground states.[31,32] Bonding analysis showed that the back-donation of Cr 3d electrons to the p_π orbitals of N_2 stabilized the HOMO a_1 orbital, which favored a closed-shell electronic structure. NBO population analysis showed that there was about 0.16e back-donation from CrO_2 to each N_2 unit. In $^3B_1$ $NNCrO_2$, CrO_2 back-donated only about 0.08e to N_2. This was a typical result of the difference between one-electron back-donation and two-electron back-donation.[32,33]

The symmetric and antisymmetric N−N and antisymmetric OCrO stretching vibrational frequencies of the $^1A_1$ $(NN)_2$-CrO_2 were predicted at 2355, 2327, and 1041 cm^{-1} with 140:381:335 relative intensities, in good agreement with the observed values.

$(NN)(O_2)CrO_2$. The 967.5 cm^{-1} band was *only* observed in the Cr + O_2/N_2 experiments, suggesting that this band was due to the reaction product of both O_2 and N_2. This band was produced on annealing at the expense of the $(O_2)CrO_2$ absorptions. It shifted to 930.8 cm^{-1} with $^{18}O_2$ and gave an antisymmetric OCrO stretching vibrational isotopic $^{16}O/^{18}O$ ratio of 1.0394. This band was tentatively assigned to the $(NN)(O_2)$-CrO_2 molecule. The symmetric OCrO stretching vibration was overlapped by the strong CrO_2 absorption at 965.3 cm^{-1}. In the Cr + $^{18}O_2/N_2$ spectra, a 917.6 cm^{-1} band went together with the 930.8 cm^{-1} band and probably was due to the symmetric OCrO stretching of the $(NN)(O_2)Cr^{18}O_2$ molecule. As shown in Figure 6, our DFT calculations predicted a $^1A'$ ground state $(NN)(O_2)CrO_2$. The antisymmetric and symmetric OCrO stretching vibrational frequencies were calculated at 1066 and 1056 cm^{-1} with 211:151 relative intensities. The N−N and O−O stretching frequencies were calculated to be 2465 and 1004 cm^{-1} with much lower intensities (0.3 and 66 km/mol). The observed isotopic $^{16}O/^{18}O$ ratio of antisymmetric OCrO stretching vibration of $(NN)(O_2)CrO_2$ (1.0394) was slightly higher than the isotopic ratios of the CrO_2 (1.0389), $NNCrO_2$

(1.0389), and $(NN)_2CrO_2$ (1.0386). This indicated that the OCrO angle in $(NN)(O_2)CrO_2$ was slightly more acute than that in CrO_2, $NNCrO_2$, and $(NN)_2CrO_2$ molecules, which was in good agreement with DFT calculations. As shown in Figure 6, the OCrO bond angle of $(NN)(O_2)CrO_2$ was predicted to be 112.8°, smaller than that of CrO_2 (132.0°), $NNCrO_2$ (128.7°), and $(NN)_2CrO_2$ (126.6°).

Laser ablation of a CrO_3 target produced CrO_3 molecules (observed at 968.4 cm^{-1}). However, no evidence was found for any N_2-CrO_3 complexes. DFT calculations predicted a stable $^1A_1$ ground-state $NNCrO_3$ with a strong doubly degenerate antisymmetric OCrO stretching vibration at 1058 cm^{-1}, red-shifted about 19 cm^{-1} from the CrO_3 absorption.

Binding Energy. Recent calculations showed that the B3LYP functional can provide very reliable predictions of structures and vibrational frequencies as well as binding energies of transition metal compounds.[34,35] The binding energy of NNCrO with respect to $CrO(^5\Pi) + N_2(^1\Sigma_g^+)$ was calculated to be 10.1 kcal/mol, after zero point energy correction. The binding energy for the second N_2 to CrO was estimated to be 10.4 kcal/mol, almost equal to the first N_2 binding energy, as expected for an electrostatic bonding mechanism. The binding energy of $NNCrO_2$ with respect to CrO_2 $(^3B_1) + N_2$ was predicted to be 15.7 kcal/mol. The $^1A_1$ $(NN)_2CrO_2$ was more strongly bound than $NNCrO_2$. The binding energy per N_2 was estimated to be 22.5 kcal/mol with respect to CrO_2 $(^1A_1) + 2N_2$. For comparison, we calculated the binding energy of singlet $NNCrO_2$ to be 23.5 kcal/mol (The optimized singlet $NNCrO_2$ geometry: R_{Cr-O}, 1.587 Å; ∠OCrO, 126.8°; R_{Cr-N}, 1.965 Å; R_{N-N}, 1.104 Å; ∠CrNN, 175.7°; the CrNN plane bisects the OCrO plane). Finally, the binding energy of the $^1A_1$ $NNCrO_3$ molecule was estimated to be 19.3 kcal/mol.

Reaction Mechanism. Laser ablation of a CrO_3 target produced CrO_3, CrO_2, CrO, and two Cr_2O_2 isomers. The $(NN)_xCrO$ and $(NN)_xCrO_2$ ($x = 1,2$) molecules were formed by reactions between N_2 and CrO or CrO_2, reactions 1−4, which were calculated to be exothermic. The $(NN)_xCrO$ and $(NN)_xCrO_2$ absorptions increased on annealing, suggesting that these reactions require negligible activation energy.

$$CrO\ (^5\Pi) + N_2 \rightarrow NNCrO(^5A') \qquad \Delta E = -10.1\ \text{kcal/mol} \quad (1)$$

$$NNCrO\ (^5A') + N_2 \rightarrow (NN)CrO_2\ (^5B_2) \qquad \Delta E = -10.4\ \text{kcal/mol} \quad (2)$$

$$CrO_2\ (^3B_1) + N_2 \rightarrow NNCrO_2\ (^3B_1) \qquad \Delta E = -15.7\ \text{kcal/mol} \quad (3)$$

$$NNCrO_2\ (^3B_1) + N_2 \rightarrow (NN)_2CrO_2\ (^1A_1) \qquad \Delta E = -5.4\ \text{kcal/mol} \quad (4)$$

The $Cr + O_2/N_2$ experiments are of particular interest. Co-condensation of laser-ablated Cr atoms with $O_2 + N_2$ in excess argon produced the CrO_2 and $(O_2)CrO_2$ absorptions, but no $(NN)CrO_2$ absorptions. These results might imply that CrO_2 was more easily ligated with O_2 than N_2 in the gas phase. The binding energy of $(O_2)CrO_2$ with respect to $CrO_2(^3B_1) + O_2(^3\Sigma_g^-)$ was predicted to be 40.3 kcal/mol, significantly higher than the binding energy of $NNCrO_2$ (15.7 kcal/mol), and the N_2 could be easily replaced by O_2 in the gas phase. However, the $(NN)CrO_2$, $(NN)_2CrO_2$, and $(NN)(O_2)CrO_2$ absorptions were produced on sample annealing. Both N_2 and O_2 are mobile on annealing, they can diffuse in solid argon and then react with CrO_2. The reaction may be mainly determined by diffusion rate, and the replacement reaction has low efficiency.

In the $Cr + N_2O$ experiment, the NNCrO molecule was formed by insertion reaction 5, which was predicted to be exothermic by about 68.6 kcal/mol. The NNCrO absorption increased on broadband photolysis, suggesting that this reaction probably required some activation energy.

$$Cr\ (^7S) + NNO\ (^1\Sigma^+) \rightarrow NNCrO\ (^5A') \qquad \Delta E = -68.6\ \text{kcal/mol} \quad (5)$$

The $NNCrO_2$ and $(NN)_2CrO_2$ absorptions increased on annealing, these molecules were mostly formed by reactions 6 and 7, which were predicted to be highly exothermic:

$$CrO\ (^5\Pi) + NNO\ (^1\Sigma^+) \rightarrow NNCrO_2\ (^3B_1) \qquad \Delta E = -93.1\ \text{kcal/mol} \quad (6)$$

$$NNCrO\ (^5A') + NNO\ (^1\Sigma^+) \rightarrow (NN)_2CrO_2(^1A_1) \qquad \Delta E = -88.3\ \text{kcal/mol} \quad (7)$$

Conclusions

Chromium oxide−dinitrogen complexes: $(NN)_xCrO$ and $(NN)_xCrO_2$ ($x = 1, 2$) have been prepared and isolated in solid argon by three different methods: (1) co-condensation of the CrO and CrO_2 molecules generated from laser ablation of CrO_3 with N_2/Ar, (2) reactions of laser-ablated Cr atoms with O_2/N_2/Ar mixtures, and (3) reactions of laser-ablated Cr atoms with N_2O/Ar. These complexes were identified by isotopic substitutions and density functional theoretical calculations. The results indicate that N_2 is end-on bonded to the chromium metal center in these complexes. Evidence is also presented for the $(NN)(O_2)CrO_2$ molecule. The binding energies for $(NN)_xCrO$ and $(NN)_xCrO_2$ ($x = 1, 2$) were also computationally estimated. The identification of these simple transition metal oxo−dinitrogen complexes could serve as model compounds for these classes of complexes.

Acknowledgment. We gratefully acknowledge support from NSFC (Grant No.20003003) and the Chinese NKBRSF.

References and Notes

(1) Howard, J. B.; Rees, D. C. *Chem. Rev.* **1996**, *96*, 2965.
(2) Burgess, B. K.; Lowe, D. J. *Chem. Rev.* **1996**, *96*, 2983.
(3) Hidai, M.; Mizobe, Y. *Chem. Rev.* **1995**, *95*, 1115.
(4) Richards, R. L. *Coord. Chem. Rev.* **1996**, *154*, 83.
(5) Hidai, M. *Coord. Chem. Rev.* **1999**, *185−186*, 99.
(6) Siegbahn, P. E. M.; Blomberg, M. R. A. *Chem. Rev.* **2000**, *100*, 421.
(7) Burdett, J. K.; Graham, M. A.; Turner, J. J. *J. Chem. Soc., Dalton Trans.* **1972**, 1620.
(8) DeVore, T. C. *Inorg. Chem.* **1976**, *15*, 1315.
(9) Andrews, L.; Bare, W. D.; Chertihin, G. V. *J. Phys. Chem. A* **1997**, *101*, 8417.
(10) Martinez, A. *J. Phys. Chem. A* **1998**, *102*, 1381.
(11) Sellmann, D.; Maisel, G. Z. *Naturforsch.* **1972**, *27B*, 465.
(12) Turner, J. J.; Simpson, M. B.; Poliakoff, M.; Maier, W. B.; Graham, M. A. *Inorg. Chem.* **1983**, *22*, 911.
(13) Anderson, S. N.; Richards, R. L.; Hughes, D. L. *J. Chem. Soc., Dalton Trans.* **1986**, 245.
(14) Ehlers, A. W.; Dapprich, S.; Vyboishchikov, S. F.; Frenking, G. *Organometallics* **1996**, *15*, 105.
(15) Zhou, M. F.; Zhang, L. N.; Chen, M. H.; Zheng, Q. K.; Qin, Q. Z. *J. Phys. Chem. A* **2000**, *104*, 10159.
(16) Chen, M. H.; Zhou, M. F.; Zhang, L. N.; Qin, Q. Z. *J. Phys. Chem. A* **2000**, *104*, 8627.
(17) Zhang, L. N.; Zhou, M. F.; Chen, M. H.; Qin, Q. Z. *Chem. Phys. Lett.* **2000**, *325*, 447.

(18) Chen, M. H.; Wang, X. F.; Zhang, L. N.; Yu, M.; Qin, Q. Z. *Chem. Phys*. **1999**, *242*, 81.

(19) Frisch, M. J.; Trucks, G. W.; Schlegel, H. B.; Scuseria, G. E.; Robb, M. A.; Cheeseman, J. R.; Zakrzewski, V. G.; Montgomery, J. A., Jr.; Stratmann, R. E.; Burant, J. C.; Dapprich, S.; Millam, J. M.; Daniels, A. D.; Kudin, K. N.; Strain, M. C.; Farkas, O.; Tomasi, J.; Barone, V.; Cossi, M.; Cammi, R.; Mennucci, B.; Pomelli, C.; Adamo, C.; Clifford, S.; Ochterski, J.; Petersson, G. A.; Ayala, P. Y.; Cui, Q.; Morokuma, K.; Malick, D. K.; Rabuck, A. D.; Raghavachari, K.; Foresman, J. B.; Cioslowski, J.; Ortiz, J. V.; Baboul, A. G.; Stefanov, B. B.; Liu, G.; Liashenko, A.; Piskorz, P.; Komaromi, I.; Gomperts, R.; Martin, R. L.; Fox, D. J.; Keith, T.; Al-Laham, M. A.; Peng, C. Y.; Nanayakkara, A.; Gonzalez, C.; Challacombe, M.; Gill, P. M. W.; Johnson, B.; Chen, W.; Wong, M. W.; Andres, J. L.; Gonzalez, C.; Head-Gordon, M.; Replogle, E. S.; Pople, J. A. *Gaussian 98*, revision A.7; Gaussian, Inc.: Pittsburgh, PA, 1998.

(20) Becke, A. D. *J. Chem. Phys.* **1993**, *98*, 5648.

(21) Lee, C.; Yang, E.; Parr, R. G. *Phys. Rev. B* **1988**, *37*, 785.

(22) McLean, A. D.; Chandler, G. S. *J. Chem. Phys*. **1980**, *72*, 5639. Krishnan, R.; Binkley, J. S.; Seeger, R.; Pople, J. A. *J. Chem. Phys*. **1980**, *72*, 650.

(23) Wachter, J. H. *J. Chem. Phys.* **1970**, 52, 1033. Hay, P. J. *J. Chem. Phys*. **1977**, *66*, 4377.

(24) Reed, A. E.; Curtiss, L. A.; Weinhold, F. *Chem. Rev*. **1988**, *88*, 899.

(25) Almond, M. J.; Hahne, M. *J. Chem. Soc., Dalton Trans.* **1988**, 2255.

(26) Chertihin, G. V.; Bare, W. D.; Andrews, L. *J. Chem. Phys*. **1997**, *107*, 2798.

(27) Zhou, M. F.; Andrews, L. *J. Chem. Phys*. **1999**, *111*, 4230.

(28) Chertihin, G. V.; Andrews, L. *J. Chem. Phys*. **1998**, *108*, 6404. Zhou, M. F.; Hacaloglu, J.; Andrews, L. *J. Chem. Phys*. **1999**, *110*, 9450.

(29) Huber, K. P.; Herzberg, G. *Molecular Spectra and Molecular Structure IV. Constants of Diatomic Molecules*; Van Nostrand: Toronto, 1979.

(30) Bauschlicher, C. W., Jr.; Maitre, P. *Theor. Chim. Acta* **1995**, *90*, 189.

(31) Souter, P. F.; Andrews, L. *J. Am. Chem. So*c. **1997**, *119*, 7350.

(32) Zhou, M. F.; Zhang, L. N.; Shao, L. M.; Qin, Q. Z. To be published.

(33) Maitre, P.; Bauschlicher, C. W., Jr. *J. Phys. Chem*. **1995**, *99*, 6836.

(34) Bauschlicher, C. W., Jr.; Ricca, A.; Partridge, H.; Langhoff, S. R. In *Recent Advances in Density Functional Theory*; Chong, D. P., Ed.; World Scientific Publishing: Singapore, 1997; Part II.

(35) Siegbahn, P. E. M. Electronic Structure Calculations for Molecules Containing Transition Metals. *Adv. Chem. Phys*. **1996**, XCIII.